journal

J. Am. Ceram. Soc., 75 [4] 958–63 (1992)

Subcritical Crack Growth of Macrocracks in Alumina with *R*-Curve Behavior

Theo Fett and Dietrich Munz

Kernforschungszentrum Karlsruhe, Institut für Materialforschung II, Karlsruhe 1, Germany

Subcritical crack growth of macroscopic cracks in two Al_2O_3 ceramics is investigated with single-edge-notched bending specimens under constant load. The resulting v-K_I-curves are in complete contrast to the behavior of natural cracks. In spite of the monotonic increase of the externally applied stress intensity factor due to crack extension, the crack growth rates first decrease. This behavior is caused by crack shielding due to crack border interaction and can be described by a rising crack growth resistance. Two methods are applied to determine the *R*-curve under subcritical crack growth conditions. [Key words: alumina, crack growth, R curve, bending, fracture.]

I. Introduction

THE failure of ceramic materials can be caused by subcritical crack growth of preexisting flaws until a critical dimension is attained. In the range of linear-elastic fracture mechanics, the crack growth rate da/dt is governed by the stress intensity factor K_I

$$\frac{da}{dt} = v(K_I) \tag{1}$$

where K_I describes the stresses near the crack tip and is generally written as

$$K_I = \sigma\sqrt{aY} \tag{2}$$

where σ is the applied stress, a the crack size, and Y a geometric correction factor dependent on the shape of the crack and the component.

The relation between crack growth rate and stress intensity factor can be determined by applying a load to specimens with macrocracks and measuring the crack growth directly or indirectly from the change of the compliance of the specimens. Other methods are using specimens with natural flaws, applying indirect fracture mechanics methods to obtain the da/dt–K_I relation.

Assuming a power-law relation between da/dt and K_I,

$$\frac{da}{dt} = AK_I^n = A^*\left(\frac{K_I}{K_{Ic}}\right)^n \tag{3}$$

the parameters A (or A^*) and n can be obtained from the experimentally obtained relation between the fracture stress and the loading rate[1] or from the relation between lifetime and stress. A modified lifetime method which does not require the assumption of a power law was developed by the authors.[2]

It was shown by several authors[3–6] that discrepancies can occur between results from specimens with macrocracks and from specimens with natural flaws. This behavior can be related to the increase in crack growth resistance with increasing crack extension, commonly characterized as R-curve behavior.[4,6–12] There are three main effects which can lead to a rising R-curve: interaction of the crack borders in the wake of the advancing crack, transformation in front of the advancing crack, and an increase in the size of the process zone due to microcracking.

An increase in the crack growth resistance with increasing crack extension can lead to a decrease in the crack growth rate with increasing applied stress intensity factor.[6,9,12] For the crack wake effect, Lathabai and Lawn[8] and Fett and Munz[11,13] calculated the effect of the crack interaction forces on stress intensity factor at the crack tip and the effect on the lifetime.

In this paper, results of crack growth measurements for alumina from specimens with macro- and microcracks are compared. From the results, the crack growth resistance curve is evaluated.

II. Experimental Procedure

Two commercially available materials have been investigated:

(1) 99.6% Al_2O_3 from Friedrichsfeld AG, Mannheim, FRG (Frialit/Degussit Al23)— in the following called material I. The mechanical properties are: Weibull parameter obtained from bending tests, $m = 11$, $\sigma_0 = 240$ MPa, $K_{Ic} = 3.3$ MPa·m$^{1/2}$. The average grain size is 20 μm.

99.6% Al_2O_3 (HIPed) from ASEA, Sweden—in the following called material II. Weibull parameter obtained from bending tests, $m = 10.4$, $\sigma_0 = 370$ MPa, $K_{Ic} = 4$ MPa·m$^{1/2}$. This material shows an inhomogeneous grain size distribution with a mean grain size of 3.2 μm and maximum grains of $\approx$25 μm grain size.

The tests with macrocracks were performed with single-edge-notched specimens of size 3.5 × 4.5 × 50 mm. The notch in the center of the specimen was prepared with a diamond saw. The notch depth was 2.245 ± 0.01 mm, the notch width 50 μm. The specimens were loaded in three-point bending with a constant load P. The distance of the loading rollers was 45 mm. The tests have been performed at room temperature in normal air environment for material I and in water for material II.

The time-dependent displacement δ was measured as shown in Fig. 1 in the center of the specimen. For some tests, the crack length was also measured at the surface, using a traveling microscope. It was observed that immediately after load application several cracks developed simultaneously. After some crack extension, only one of them continued to propagate.

In Table I, the outer fiber stress of the unnotched specimen σ— as a measure of the applied load—and the initial stress intensity factor K_{Ii} are given. The numbers refer to the curves in Figs. 4, 5, 8, and 9.

The tests with specimens containing natural flaws were obtained from the scatter of the lifetime of tests with constant load applying the modified lifetime method.[2] The results represent the initial crack growth rate of natural cracks at the beginning of a constant load test. The details of the evalu-

B. R. Lawn—contributing editor

Manuscript No. 197047. Received December 26, 1990; approved December 9, 1991.

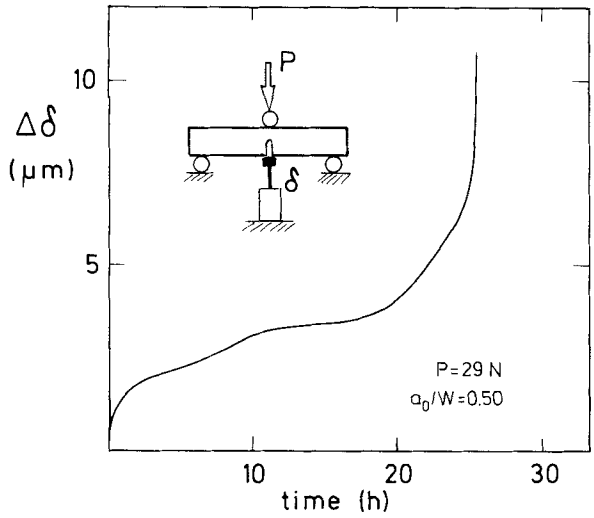

Fig. 1. Displacement vs time curve for a static test carried out with SENB specimen (50-μm saw cut) in three-point bending test.

ation are published elsewhere.[14,15] Here only the final results are reported.

III. Experimental Results and Data Evaluation

An example of the change of the displacement $\Delta\delta$ with time is shown in Fig. 1. The general trend is first a decrease in the displacement rate $d\Delta\delta/dt$ and a steep increase before final fracture. In some specimens with low loads, crack arrest was observed. From the displacement, the crack length a, and from the crack length a, the stress intensity factor K_I, were calculated.

(I) Determination of Crack Length

In a first approximation, the crack length has been evaluated by linear-elastic analysis from the compliance, neglecting the effect of R-curve.

The compliance

$$C = \frac{\delta}{P} \tag{4}$$

consists of the compliance of the uncracked bar C_0 and the portion ΔC caused by the crack.

$$C = C_0 + \Delta C \tag{5}$$

with

$$C_0 = \frac{L^2}{W^2BE}\left[\frac{L}{4W} + \frac{(1+\nu)W}{2L}\right] \tag{6}$$

where E is Youngs modulus, ν is Poisson's ratio, W is the specimen width, B is the specimen thickness, and L is the supporting roller span. The compliance part due to the crack can be

Table I. Loading Conditions for the Test Specimens

Material	Specimen	σ (MPa)	K_{Ii} (MPa·m$^{1/2}$)
I	1	22.2	2.72
I	2	24.0	2.96
I	3	25.0	3.06
I	4	23.0	2.82
I	5	26.2	3.20
I	6	26.3	3.21
I	7	26.6	3.25
II	1	24.0	2.93
II	2	26.5	3.25
II	3	26.9	3.32
II	4	31.5	3.85

Table II. Coefficients for Eq. (7)

	B_{i0}	B_{i1}	B_{i2}	B_{i3}
$i = 0$	1.9634	−0.6473	−0.4645	1.4479
$i = 1$	−5.9080	−0.5307	1.8855	−4.3890
$i = 2$	10.9909	6.2296	−2.3368	3.2163
$i = 3$	−13.130	−12.356	0.08942	3.34771
$i = 4$	8.7702	11.3087	1.7797	−6.3733
$i = 5$	−2.4832	−4.0318	−0.9616	2.7738

obtained for any ratio $W/L \geq 2$ from Ref. 16 as

$$\Delta C = \frac{9}{2}\frac{L^2}{W^2EB}\left(\frac{\alpha}{1-\alpha}\right)^2 \sum_{i=0}^{5}\sum_{j=0}^{3} B_{ij}\alpha^i(W/L)^j \tag{7}$$

with $\alpha = a/W$. The coefficients B_{ij} are given in Table II.

In Fig. 2, the change in the crack length Δa_{comp} obtained from the change of the compliance with time is plotted versus the optically measured length of the dominating crack Δa_{opt} for a specimen with a load corresponding to an initial stress intensity factor of $K_{Ii}/K_{Ic} = 0.8$. For small Δa, the compliance method leads to an overestimation, and for larger Δa, to an underestimation of the optically measured crack length. This behavior is in agreement with measurements reported by Hübner and Jillek.[17]

The overestimation could result from the development of several small cracks shortly after load application. The underestimation obviously is related to crack border interactions leading to the R-curve behavior as described in Section V.

Although the real crack length cannot be obtained exactly with the compliance method, this method shows some important advantages over the optical crack size measurement:

(1) While the compliance method yields monotonically increasing crack length data, the optical crack length measurement with the traveling microscope provides the crack length only in discrete time steps.

(2) The compliance method is not restricted to the specimen surfaces and yields a mean value of the crack length which is representative of the whole specimen thickness.

(3) The compliance can be determined with a very high resolution.

(4) At high temperatures, the visual determination of crack length becomes very complicated. Displacement measurements can be made conveniently at high temperatures, too.

The most appropriate procedure seems to be to combine the two methods. Direct observation of the crack tip location in longer time steps, together with the continuously recorded

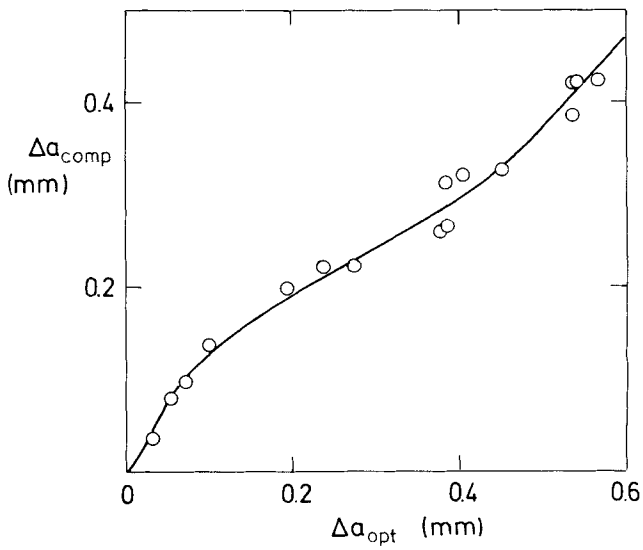

Fig. 2. Interdependency of crack size from compliance measurements and crack size measured with a traveling microscope.

Table III. Coefficients for Eq. (9)

	A_{i0}	A_{i1}	A_{i2}	A_{i3}	A_{i4}
$i = 0$	1.1200	−0.2387	0.4317	−1.7351	2.4145
$i = 1$	−1.8288	−0.2573	−4.9847	16.9047	−18.2883
$i = 2$	2.9741	0.2706	18.6767	−60.4912	59.9239
$i = 3$	−2.4280	0.5627	−27.3447	87.7078	−85.2405
$i = 4$	0.6712	−0.5184	13.5837	−43.5421	42.3503

displacements in the load line, provides all information necessary to determine v–K-curves.

(2) Determination of Stress Intensity Factors

The geometric function Y for three-point bending with the reference stress

$$\sigma_0 = \frac{3}{2}\frac{PL}{W^2B} \tag{8}$$

has been determined in Ref. 16 for $L/W > 2$ using the weight functions method

$$Y = \frac{\sqrt{\pi}}{(1-\alpha)^{3/2}}\left[0.3738\alpha + (1-\alpha)\sum_{i,j=0}^{4} A_{ij}\alpha^i (W/L)^j\right] \tag{9}$$

with the coefficients given in Table III.

(3) da/dt–K_I-Curves

The crack growth rate da/dt was obtained from the $a(t)$-curve as the secant value $[a(t + \Delta t) - a(t)]/\Delta t$. The stress intensity factor $[K_I(t + \Delta t) + K_I(t)]/2$ obtained from Eq. (2) is called $K_{I\,appl}$.

Figure 3 shows a plot of a da/dt–$K_{I\,appl}$-curve for material I obtained from a_{comp} compared with an evaluation using a_{opt} (obtained by the procedure described in Section III(1)) for da/dt as well as for $K_{I\,appl}$. The fracture toughness obtained from four-point-bending tests with a saw cut of 50 μm width (SENB) is introduced in order to show that the stress intensity factors $K_{I\,appl}$ occurring in the static tests can be significantly higher than the "fracture toughness." The general trend for the curves obtained from a_{comp} and a_{opt} is the same and the differences in the curves are very small.

In Fig. 4, da/dt–$K_{I\,appl}$-curves for different applied stresses are plotted with the crack length obtained from a_{comp}. Two typical types of da/dt–K_I-curves can be seen. Tests with low initial stress intensity factors show first a decrease of the crack growth rate with increasing crack length and therefore increasing $K_{I\,appl}$. The crack growth rate drops by several orders of magnitude within a small amount of crack extension. After a large range with nearly constant crack growth rate, the crack growth rate increases until final fracture. For the lowest K_{Ii} (curve 1), crack arrest was observed. Cracks starting with a high initial stress intensity factor K_{Ii} (caused by a higher load applied) exhibit an approximatively constant crack growth rate until an increase to final fracture. The arrows at the curve ends indicate that the curves continue in principle but that no correct measurement was possible. In case of crack arrest, the crack velocities become unmeasurably low, and directly before fracture the crack velocities become unmeasurably high.

Figure 4 also contains the results of tests with natural cracks from Ref. 14. These results can be described by Eq. (3) with $A^* = 5 \times 10^{-4}$ m/s, $n = 38.6$.

It can be seen that the initial values of the tests with the specimens with macrocracks are near the curve for the specimens with natural flaws.

The da/dt–K_I-curves obtained for material II are plotted in Fig. 5. The specimens with macrocracks show the same behavior as for material I. Again results from the specimens with natural flaws from a previous publication[15] are shown, which can be described by Eq. (3) with $A^* = 5 \times 10^{-4}$ m/s, $n = 19$. In addition, a da/dt–K_I-curve determined with the double-torsion method[18] is shown in Fig. 5. The n value of this investigation is 210, in complete contrast to the results obtained with natural cracks.

In one of the tests, crack arrest occurred. After an increase in load, the crack started again (Fig. 6), and a second crack arrest was observed.

It is interesting to see in Figs. 4 and 5 that the macrocracks are extending beyond $K_{I\,appl} = K_{Ic}$.

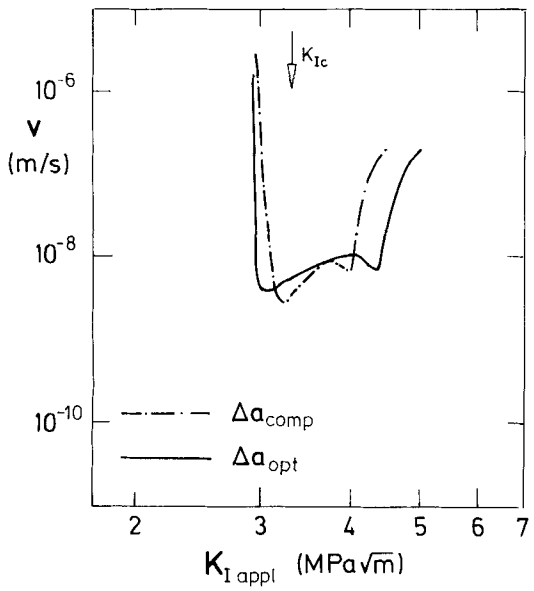

Fig. 3. v–$K_{I\,appl}$-curve evaluated on the basis of compliance measurements compared with the v–$K_{I\,appl}$-curve on the basis of directly measured crack lengths.

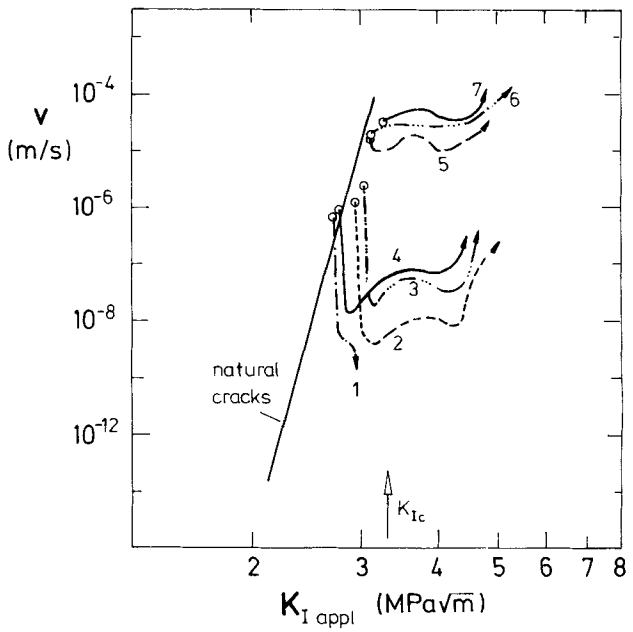

Fig. 4. v–$K_{I\,appl}$-curves for material I specimens with saw cuts compared with subcritical crack growth behavior of small cracks. Numbers refer to Table I.

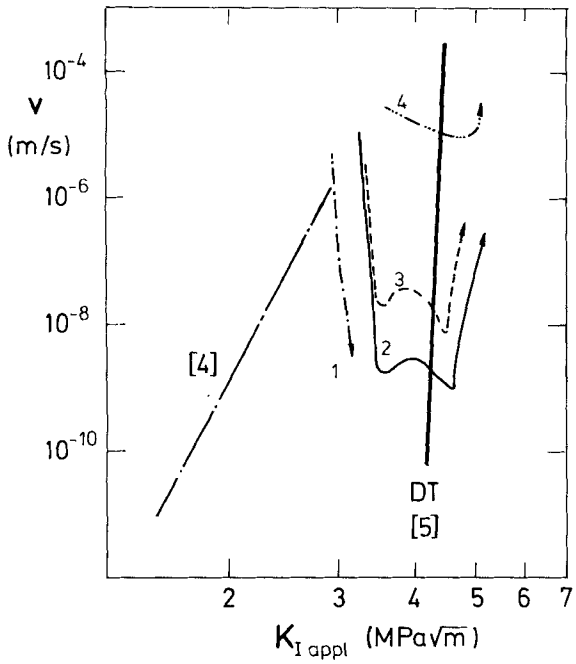

Fig. 5. v–$K_{I\,appl}$-curves for material II specimens with saw cuts compared with subcritical crack growth behavior of small cracks.

IV. Discussion

From the three effects mentioned in the introduction, which can cause an R-curve effect, the crack border interaction is assumed to be responsible for the investigated material, as was shown for especially coarse-grained Al_2O_3.[20–25] The stress intensity factor acting at the crack tip $K_{I\,tip}$ is composed of the stress intensity factor caused by the external load, calculated for interaction-free crack faces $K_{I\,appl}$ and K_{Is} caused by the interaction forces. K_{Is} is called the shielding stress intensity factor:[26]

$$K_{I\,tip} = K_{I\,appl} - K_{Is} \tag{10}$$

For a rapid loading test, K_{Is} increases with increasing crack extension up to a plateau value. For a test with constant load, K_{Is} can also increase.

The relation between K_{Is}, the crack extension, and the applied load can be calculated assuming a relation between the interaction forces and the crack opening displacement.[8,27,28] Here the relation between K_{Is} and the crack extension is evaluated from the crack growth rate tests applying two different methods.

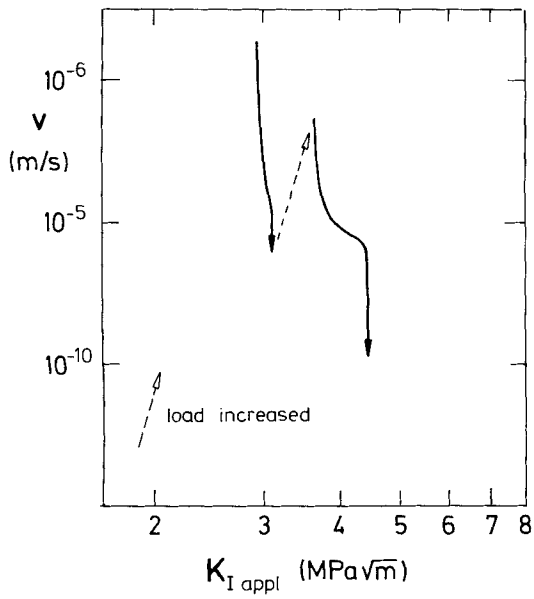

Fig. 6. v–$K_{I\,appl}$-curves for material II specimens with crack arrest.

(I) Determination of R-Curve Using the V–K Data of Natural Cracks

The first method is schematically explained in Fig. 7. The v–$K_{I\,appl}$-curve obtained in a constant load test may be represented by the solid curve in Fig. 7(a), and the natural crack results are given by the dash-dotted straight line. For a given crack growth rate (e.g., v_1) three stress intensity factors are related. In case of the subcritical crack growth rate v_1 we find the point A_1 corresponding to the subcritical crack growth of the natural cracks. The corresponding stress intensity factor is assumed to be the crack tip stress intensity factor $K_{I\,tip}$ that is given according to Eq. (9) by

$$K_{I\,tip} = K_{Ic}\left(\frac{da/dt}{A^*}\right)^{1/n} \tag{11}$$

On the decreasing part of the macrocrack curve, the intersection of the curve with $v = v_1$ is B_1, and after longer crack propagation the crack growth velocity reaches once more the crack growth rate v_1. This situation is marked by C_1. For the lower crack growth rate v_2, the corresponding points are A_2, B_2, C_2. The shielding stress intensity factors K_{Is} corresponding to the different crack extensions at points B_1, B_2, C_1, C_2 are given by

$$K_{Is} = K_{I\,appl} - K_{Ic}\left(\frac{da/dt}{A^*}\right)^{1/n} \tag{12}$$

The R-curve resulting from the macrocrack data given in Fig. 7(a) is illustrated in Fig. 7(b).

Figure 8 shows the resulting K_{Is}–Δa-curves based on the data represented in Fig. 4. An increase in K_{Is} with increasing crack extension is observed. The initial K_{Ii} has an effect on the shape of the curve. For small values of K_{Ii}, first a rapid increase in K_{Is} is observed. For larger values of K_{Ii}, this first

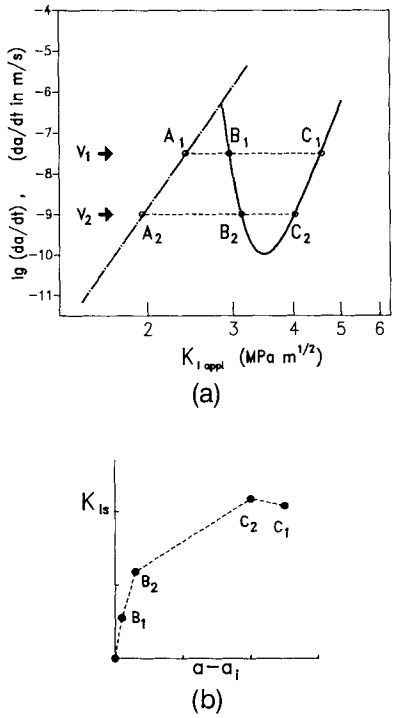

Fig. 7. Determination of the shielding stress intensity factor K_{Is} (schematically); (a) v–K_I curves for natural cracks (dash-dotted line) and macrocracks (solid line); (b) corresponding R-curve ($K_{Is} = f(\Delta a)$)

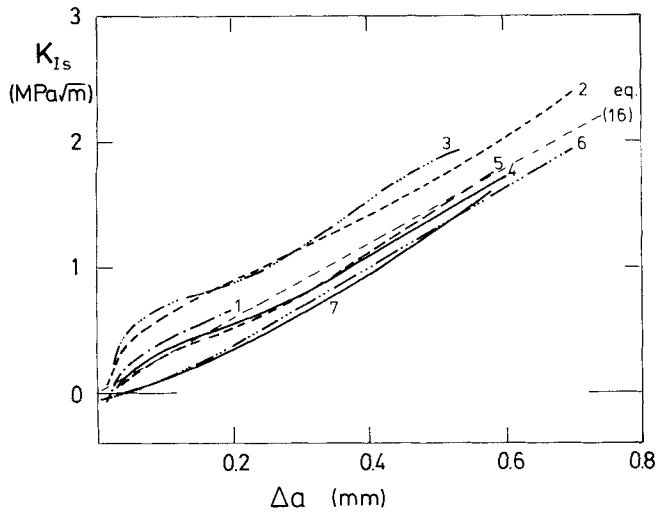

Fig. 8. R-curves K_I vs Δa for material I.

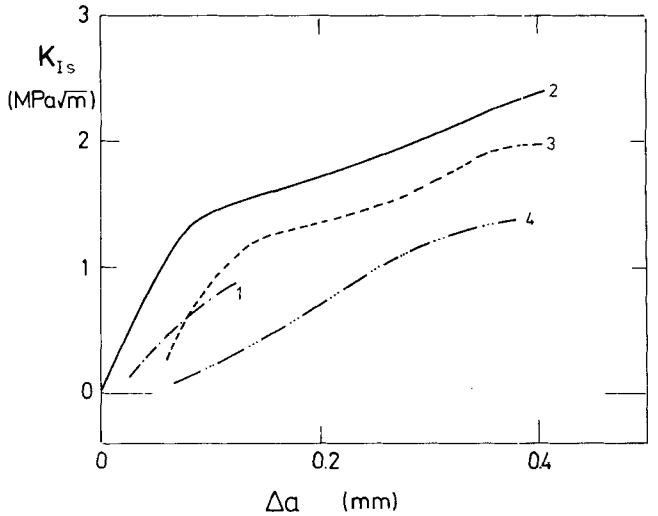

Fig. 9. R-curves K_{Is} vs Δa for material II.

increase is smaller. It should be kept in mind, however, that $K_{I\,tip}$ is not constant for one curve. As a tendency, one observes that the curves 1 to 4—corresponding to the lower crack growth rates—exhibit higher values of K_{Is}.

The mean R-curve resulting from all the data of Fig. 8 can be described by

$$\overline{K_{Is}} = 3.15 \frac{\text{MPa}\sqrt{\text{m}}}{\text{mm}} \Delta a \qquad (13a)$$

The upper limit curve can be expressed by

$$K_{Isu} = 3.15 \frac{\text{MPa}\sqrt{\text{m}}}{\text{mm}} \Delta a + 0.35 \frac{\text{MPa}\sqrt{\text{m}}}{\text{mm}} \tanh \frac{\Delta a}{0.03\ \text{mm}} \qquad (13b)$$

Figure 9 shows the R-curve $K_{Is}(\Delta a)$ for material II. In principle, material II exhibits the same R-curve effects (and subcritical crack growth behavior) as material I.

(2) Determination of Parameters for a Prescribed Type of R-Curve

A further possibility of determining the R-curve from the combined results of specimens with macrocracks and natural flaws as shown in Fig. 4 is to fit the measured data with a prescribed type of R-curve law and to determine the best set of parameters by a least-squares procedure.

A simple R-curve description with two parameters is given in Ref. 13:

$$K_{Is} = \begin{cases} K_{Is\,max}\left[2\frac{\Delta a}{\Delta a_1} - \left(\frac{\Delta a}{\Delta a_1}\right)^2\right] & \text{for} \quad \Delta a/\Delta a_1 \le 1 \\ K_{Is\,max} & \text{for} \quad \Delta a/\Delta a_1 > 1 \end{cases} \qquad (14)$$

Assuming a power law, the subcritical crack growth rate can be written

$$v = \frac{A^*}{K_{Ic}^n}[K_{I\,appl} - K_{Is}(\Delta a)]^n \qquad (15)$$

In principle, all material parameters ($K_{Is\,max}$, Δa_1, A^*, and n) can be obtained by curve-fitting. But since the value n is known, the number of degrees of freedom can be reduced. Using the fixed n value of $n = 39$ (as obtained for the small cracks), the least-squares routine yields for the data of Fig. 4 for material I

$$K_{Is\,max} = 109.8\ \text{MPa}\sqrt{\text{m}}, \qquad \Delta a_1 = 13.47\ \text{m},$$
$$A^* = 1.5 \times 10^{-4}\ \text{m/s}$$

Since the value Δa_1 is very high compared with the measured range of crack extension $\Delta a < 0.8$ mm, a linear dependency results from Eq. (14). It is given by

$$K_{Is} = 2.96\ \text{MPa}\sqrt{\text{m}}/\text{mm}\,\Delta a \qquad (16)$$

which is in good agreement with the relation obtained in Eq. (13a). The straight line described by Eq. (16) is entered in Fig. 8 as a dashed line.

VI. Conclusions

Measurements on bending specimens of two 99.6% Al_2O_3 ceramics with large cracks were carried out in static three-point bending tests. The main results are as follows:

(1) In contrast to the results for small cracks obtained in an indirect way (determined by a lifetime procedure), the macro v–K_I-curves of the two materials showed for small crack extensions a decreasing subcritical crack growth rate with an increasing stress intensity factor applied. For large crack extensions, the crack growth rate then increases, followed by failure of the specimen.

(2) R-curves were derived in the representation $K_{Is}(\Delta) = K_{I\,appl} - K_{I\,tip}$. Monotonically increasing curves were found.

(3) For high initial stress intensity factors, both materials exhibit a nearly linear dependency $K_{Is} \propto \Delta a$ over a range of at least $\Delta a = 0.8$ mm of crack extension.

(4) The R-curves corresponding to the lower initial stress intensity factors are more pronounced and their dependency seems to be nonlinear.

(5) The comparison of the small-crack v–K curves with the results illustrated in Figs. 4 and 5 shows that it is not sufficient to characterize the crack-growth behavior of a ceramic material by macrocrack data.

References

[1]R. J. Charles, "Dynamic Fatigue of Glass," *J. Appl. Phys.*, **29**, 1657–61 (1958).

[2]T. Fett and D. Munz, "Determination of v–K_I-Curves by a Modified Evaluation of Lifetime Measurements in Static Bending Tests," *J. Am. Ceram. Soc.*, **68**, C-213–C-215 (1985).

[3]T. E. Adams, D. J. Landini, C. A. Schumacher, and R. C. Bradt, "Micro- and Macrocrack Growth in Alumina Refractories," *Am. Ceram. Soc. Bull.*, **60**, 730–35 (1981).

[4]B. J. Pletka and S. M. Wiederhorn, "A Comparison of Failure Predictions by Strength and Fracture Mechanics Techniques," *J. Mater. Sci.*, **17**, 1247–68 (1982).

[5]K. Chen and Y. Ko, "Slow Crack Growth in Silica, High Alumina, Alumina–Chromia, and Zircon Brick," *Am. Ceram. Soc. Bull.*, **67**, 1228–34 (1988).

[6]T. Fett and D. Munz, "Lifetime Evaluation of Ceramic Materials," *J. Eur. Ceram. Soc.*, **6**, 67–72 (1990).

[7]E. K. Beauchamp and S. L. Monroe, "Effect of Crack-Interface Bridging on Subcritical Crack Growth in Ferrites," *J. Am. Ceram. Soc.*, **72**, 1179–84 (1989).

[8]S. Lathabai and B. R. Lawn, "Fatigue Limits in Noncyclic Loading of Ceramics with Crack-Resistance Curves," *J. Mater. Sci.*, **24**, 4298–306 (1989).

[9]D. G. Jensen, V. Zelizko, and M.V. Swain, "Small Flaw Static Fatigue Crack Growth in Mg-PSZ," *J. Mater. Sci. Lett.*, **8**, 1154–57 (1989).

[10]A. Okada, N. Hirosaki, and M. Yoshimura, "Subcritical Crack Growth in Sintered Silicon Nitride Exhibiting a Rising *R*-Curve," *J. Am. Ceram. Soc.*, **73**, 2095–2096 (1990).

[11]T. Fett and D. Munz, "Influence of *R*-Curve Effects on Lifetimes in Static Tests," *J. Mater. Sci. Lett.*, **9**, 1471–72 (1990).

[12]T. Fett and D. Munz, "Subcritical Crack Growth of Macro-Cracks in Zirconia," *J. Mater. Sci. Lett.*, **10**, 1103–106 (1991).

[13]T. Fett and D. Munz, "Influence of *R*-Curve Effects on Lifetimes for Specimens with Natural Cracks"; in Proceedings of the Conference *Fracture Processes in Brittle Disordered Materials*, June 19–22, 1991, Noordwijk, Netherlands. Edited by J. G. M. von Mier, J. G. Rots, and A. Bakker. Chapman and Hall, London, U.K., 1991.

[14]T. Fett and D. Munz, "Static and Cyclic Fatigue of Ceramic Materials"; pp. 1827–35 in Proceedings of the 7th CIMTEC, June 24-30, 1990. Edited by P. Vincenzini. Elsevier Science Publishers B.V., 1991.

[15]T. Fett, K. Keller, and D. Munz, "Determination of Crack Growth Parameters of Alumina in 4-Point Bending Tests," NAGRA Technical Report No. 85-51, Baden, Switzerland, 1985.

[16]T. Fett, "An Analysis of the 3-Point Bending Bar by Use of the Weight Function Method," *Eng. Fract. Mech.*, **40**, 683–86 (1991).

[17]H. Hübner and W. Jillek, "Sub-Critical Crack Extension and Crack Resistance in Polycrystalline Alumina," *J. Mater. Sci.*, **12**, 117–25 (1977).

[18]W. Hermansson, "Determination of Slow Crack Growth in Isostatically Pressed Al_2O_3"; in *Aluminum Oxide as an Encapsulation Material for Unreprocessed Nuclear Fuel Waste — Evaluation from the Viewpoint of Corrosion*, Technical Report No. 80-15. KBS, Stockholm, Sweden, 1980.

[19]The Swedish Corrosion Institute and its Reference Group, *Aluminum Oxide as an Encapsulation Material for Unreprocessed Nuclear Fuel Waste–Evaluation from the Viewpoint of Corrosion*, Technical Report No. 80-15. KBS Stockholm, Sweden, 1980.

[20]R. Knehans and R.W. Steinbrech, "Memory Effect of Crack Resistance during Slow Crack Growth in Notched Al_2O_3 Bend Specimens," *J. Mater. Sci. Lett.*, **1**, 327–29 (1982).

[21]R.W. Steinbrech, R. Knehans, and W. Schaarwächter, "Increase of Crack Resistance during Slow Crack Growth in Al_2O_3 Bend Specimens," *J. Mater. Sci. Lett.*, **18**, 265–70 (1983).

[22]P. L. Swanson, C. J. Fairbanks, B. R. Lawn, Y. Mai, and B. J. Hockey, "Crack-Interface Grain Bridging as a Fracture Resistance Mechanism in Ceramics: I, Experimental Study on Alumina," *J. Am. Ceram. Soc.*, **70**, 279–89 (1987).

[23]G. Vekinis, M. F. Ashby, and P.W. R. Beaumont, "*R*-Curve Behaviour of Al_2O_3 Ceramics," *Acta Metall. Mater.*, **38**, 1151–62 (1990).

[24]H. Frei and G. Grathwohl, "New Test Methods for Engineering Ceramics—in-Situ Microscopy Investigation," *CFI, Ceram. Forum Int.*, **67**, 27–35 (1991).

[25]J. Rödel, J. F. Kelly, and B. R. Lawn, "In Situ Measurements of Bridged Crack Interfaces in the Scanning Electron Microscope," *J. Am. Ceram. Soc.*, **73**, 3313–18 (1990).

[26]B. R. Lawn, "Physics of Fracture," *J. Am. Ceram. Soc.*, **66**, 83–91 (1983).

[27]Y. Mai and B. R. Lawn, "Crack-Interface Grain Bridging as a Fracture Resistance Mechanism in Ceramics: II. Theoretical Fracture Mechanics Model," *J. Am. Ceram. Soc.*, **70**, 289 (1987).

[28]T. Fett and D. Munz, "Influence of Crack-Surface Interactions on Stress Intensity Factor in Ceramics," *J. Mater. Sci. Lett.*, **9**, 1403–406 (1990). □